Received: 5 September 2017 | Revised: 3 November 2017 | Accepted: 6 November 2017

DOI: 10.1002/jms.4048

WILEY Journal of MASS SPECTROMETRY

RESEARCH ARTICLE

Accelerated, untargeted metabolomics analysis of cutaneous T-cell lymphoma reveals metabolic shifts in plasma and tumor adjacent skins of xenograft mice

Yunchen Le[1] | Xiaoyan Shen[2] | Hongyan Kang[1] | Qizheng Wang[1] | Kejia Li[2] | Jie Zheng[2] | Yunqiu Yu[1]

[1] School of Pharmacy, Fudan University, Key Laboratory of Smart Drug Delivery, Ministry of Education, Shanghai 201203, PR China

[2] Department of Dermatology, Ruijin Hospital, School of Medicine, Shanghai Jiaotong University, Shanghai 200025, PR China

Correspondence
Yunqiu Yu, School of Pharmacy, Fudan University, Shanghai 201203, PR China.
Email: yqyu@shmu.edu.cn

Jie Zheng, Department of Dermatology, Ruijin Hospital, School of Medicine, Shanghai Jiaotong University, Shanghai 200025, PR China.
Email: jie-zheng2001@126.com

Funding information
Natural Science Foundation of China, Grant/Award Number: KRF301100

Abstract

Cutaneous T-cell lymphoma (CTCL) is a heterogeneous group of skin-homing T-cell neoplasms. Clinical management is stage based but diagnosis and prognosis could be extremely challenging. The presented study aims to explore the metabolic profiling of CTCL by an accelerated untargeted metabolomics data analysis tool "Mummichog" to facilitate the discoveries of potential biomarkers for clinical early stage diagnosis, prognosis, and treatments in CTCL. Ultra high-performance liquid chromatography–quadrupole time-of-flight–based untargeted metabolomics were conducted on the skin and plasma of CTCL mice. It showed that the metabolism of skin changed greatly versus control samples in the development of CTCL. Increased L-glutamate and decreased adenosine monophosphate were the most essential metabolic features of CTCL tumor and tumor adjacent skins. Unique metabolism changes in tumor adjacent non-involved skin tissues (ANIT) occurred in the progress of carcinogenesis, including upregulated cytidine-5′-triphosphate, aberrant biosynthesis of prostaglandins, pyrimidine, mevalonate pathway, and tryptophan degradation. Sharply elevated 5-phospho-α-D-ribose 1-diphosphate (PRPP) marked the final state of tumor in CTCL. In the plasma, systematic shifts in corticosterone, sphingolipid, and ceramide metabolism were found. These uncovered aberrant metabolites and metabolic pathways suggested that the metabolic reprogramming of PRPP in tumor tissues may cause the disturbance of cytidine and uridine metabolic homeostasis in ANIT. Accumulative cytidine-5′-triphosphate in ANIT may exert positive feedback on the PRPP level and leads to CTCL further development. In addition, the accelerated data analysis tool "Mummichog" showed good practicability and can be widely used in high-resolution liquid chromatography mass spectrometry–based untargeted metabolomics.

KEYWORDS

cutaneous T-cell lymphoma (CTCL), data analysis, metabolic pathways, metabolomics, ultra high-performance liquid chromatography–quadrupole time-of-flight mass spectrometry (UHPLC-QTOF)

1 | INTRODUCTION

Cutaneous T-cell lymphoma (CTCL) is a heterogeneous group of skin-homing T-cell neoplasms, which represent approximately 75% of all primary cutaneous lymphomas.[1] Mycosis fungoides and its leukemic variant, Sezary syndrome, are malignancies of skin-homing T-cells that comprise most CTCL.[2] Advanced-stage mycosis fungoides (stage IIB to IV) and Sezary syndrome are aggressive lymphomas with a median survival of 1 to 5 years.[3] Clinical management is stage based but

Abbreviations: ANIT, adjacent non-involved skin tissue; CoA, coenzyme A; CTCL, cutaneous T-cell lymphoma; CTP, cytidine-5′-triphosphate; DNIT, distant non-involved skin tissue; FC, fold change; GLT, L-glutamate; HRLC-MS, high-resolution liquid chromatography–mass spectrometry; NADP, nicotinamide adenine dinucleotide phosphate; PCA, principal component analysis; PLS-DA, partial least squares–discriminant analysis; PRPP, 5-phospho-α-D-ribose 1-diphosphate; ROC, receiver operating characteristic curve; S1P, sphingosine-1-phosphate; UHPLC-QTOF, ultra high-performance liquid chromatography–quadrupole time-of-flight

Yunchen Le and Xiaoyan Shen contributed equally to this work.

diagnosis may be extremely challenging because benign disorders may have overlapping features with those of lymphoma.[4] The variability of presentation and diagnostic uncertainty has still challenged clinicians confronted with CTCL.

The diagnosis of CTCL requires a more holistic approach through which molecular findings are to be integrated with clinical, histological, and immunophenotypic data. Multi-omics technique has been used in the precision medicine and personal diagnosis of CTCL in recent years, including high-throughput sequencing of T-cell receptor,[5] transcriptional profiling,[6] proteomic approaches,[7] and metabolomics investigation.[8] In the light of previous omics findings, the presented study aims to explore the pathogenesis of CTCL from metabolomics perspective using an accelerated, untargeted metabolomics data analysis strategy. We focus on the discoveries of instinctive and changing metabolic pathways involved in the carcinogenic progression of skins and plasma of CTCL. Dynamical metabolome shifts were observed by comparison of tumor-involved skins with healthy skins. Different metabolic signatures of plasma between CTCL mice and healthy mice were also investigated. The uncovered metabolic reprogramming in CTCL would help to broaden our understanding of the pathogenesis and facilitate the early stage diagnosis, prognosis, and clinical treatments of CTCL.

On the other hand, conventional metabolomics workflow involved in low throughput metabolites identification by tandem mass spectrometry or coelution of isotopically labeled known references. To accelerate the analysis and focus on the metabolic pathways, we applied a tool "Mummichog," proposed by Li et al,[9] to predict metabolic pathways networks in CTCL metabolomics research without a priori identification of metabolites, thus greatly accelerated the workflow. Mummichog is a set of algorithms specifically designed for high-resolution liquid chromatography–mass spectrometry (HRLC-MS) metabolomics by combining network analysis and metabolites prediction under the same computational framework. The application of this accelerated metabolomics data analysis strategy in this study significantly shortens the analysis time and obtains robust results by reducing the ambiguity in metabolites prediction. Our study provides new evidence for the application of this strategy in HRLC-MS–based metabolomics.

2 | EXPERIMENTAL DETAILS

2.1 | Cells and chemicals

Cell culture: RPMI 1640 medium (American Type Culture Collection ATCC 30-2001), HH cell (T-cell Lymphoma ATCC CRL-2105), penicillin streptomycin (Hyclone, SV30010, 10 000 units/mL penicillin, 10 000 units/mL streptomycin), fatal bovine serum (F2442-500 mL), and dimethyl sulfoxide (Sigma-Aldrich, St. Louis, Missouri).

Chemicals: acetonitrile, methanol (HPLC grade), and dichloromethane were purchased from Sinopharm Chemical Reagent Co, Ltd. (Shanghai, China). Formic acid (HPLC grade) was purchased from Dima Technology Inc (Lake Forest, California). The standard chemicals for metabolites identification were obtained from Sigma-Aldrich (St. Louis) and Aladdin Industrial Corporation (Shanghai, China). Distilled water was filtered through a Milli-Q system (Millipore Corporation, Billerica, Massachusetts).

2.2 | CTCL xenograft mice and sample collection

The HH cells of logarithmic growth phase were transferred from the culture flask to the centrifuge tube, and serum-free medium was added to resuspend after 130 g × 6 minutes of centrifuging. Above steps repeated to a cell concentration of about 1 × 10^7/mL, and 0.2-mL HH cells were injected subcutaneously into the right axillary of Balb/c female nude mice (n = 16). The other 5 female nude mice were subcutaneously injected of 0.2-mL sterile Phosphate Buffered Saline (PBS) as control mice. The CTCL xenograft mice model was established successfully in 2 to 3 weeks.

The CTCL tumor skin tissue (tumor), adjacent non-involved skin tissue (ANIT), distant non-involved skin tissue (DNIT), and control mice healthy skin tissue (control) were taken from right and left axillaries, respectively (Figure 1A). Then samples were quenched in liquid nitrogen. Orbital blood was collected to heparin sodium tube, and plasma samples were obtained after centrifugation at 3000 rpm for 10 minutes. All plasma samples and tissue samples were stored in −80°C.

2.3 | Sample treatment and data acquisition

Skin tissue sample treatment: skin tissue samples were thawed on dry ice, weighted, vortexed, and ultrasound in −20°C cold acetonitrile and water (1:1, v/v) (50 μL to every 1 mg of tissue) for 5 and 10 minutes, respectively. Then samples were homogenized with washed stainless beads on an electric tissue homogenizer, using a frequency of 60 Hz for 60 seconds. After that samples were vortexed for 10 seconds and stainless beads were removed. Samples were centrifuged at 9000 rpm for 10 minutes, and supernatant was added with 100-μL methanol. Next, samples were vortexed for 5 minutes and let stand for 10 minutes. After another centrifugation at 9000 rpm for 10 minutes, the supernatant was transfer to ultra high-performance liquid chromatography–quadrupole time-of-flight (UHPLC-QTOF) full-scan analysis.

In plasma sample treatment, 50-μL plasma sample was thawed at ambient temperature, and in 200 μL, −20°C cold methanol was added and vortexed for 5 minutes. Then samples were let to stand for 10 minutes and centrifuged at 12 000 rpm for 15 minutes at 4°C, and the supernatant was transferred to UHPLC-QTOF full-scan analysis.

Quality control samples were prepared by taking equal portions of each disease type and control samples and combining them.

In acquisition of data, a 5-μL aliquot of the supernatant was injected onto an Agilent UHPLC system (Infinity 1260) equipped with a UPLC ACQUITY HSS T3 column (ACQUITY HSS T3, 2.1 × 100 mm, 1.8 μm, Waters Corporation, Milford, Massachusetts) at a column temperature of 35°C. The UHPLC system was coupled to an Agilent 6520 electrospray ion source Accurate-Mass QTOF (Agilent Technologies, Santa Clara, California). The flow rate was 0.3 mL/min, and the mobile phase was water consisted of 0.1% formic acid solution (A) and acetonitrile containing 0.1% formic acid (B), respectively. The linear gradient conditions were set as follows: time (t) = 0-1 minutes, hold B at 1%; t = 1-5 minutes, increase B from 1% to 40%; t = 5-8 minutes, increase B from 40% to 50%; t = 8-10 minutes, increase B from 50% to 65%; t = 10-16 minutes, increase B from 65% to 76%; t = 16-20 minutes, increase B from 76% to 100%; t = 20-25 minutes hold B at 100%;

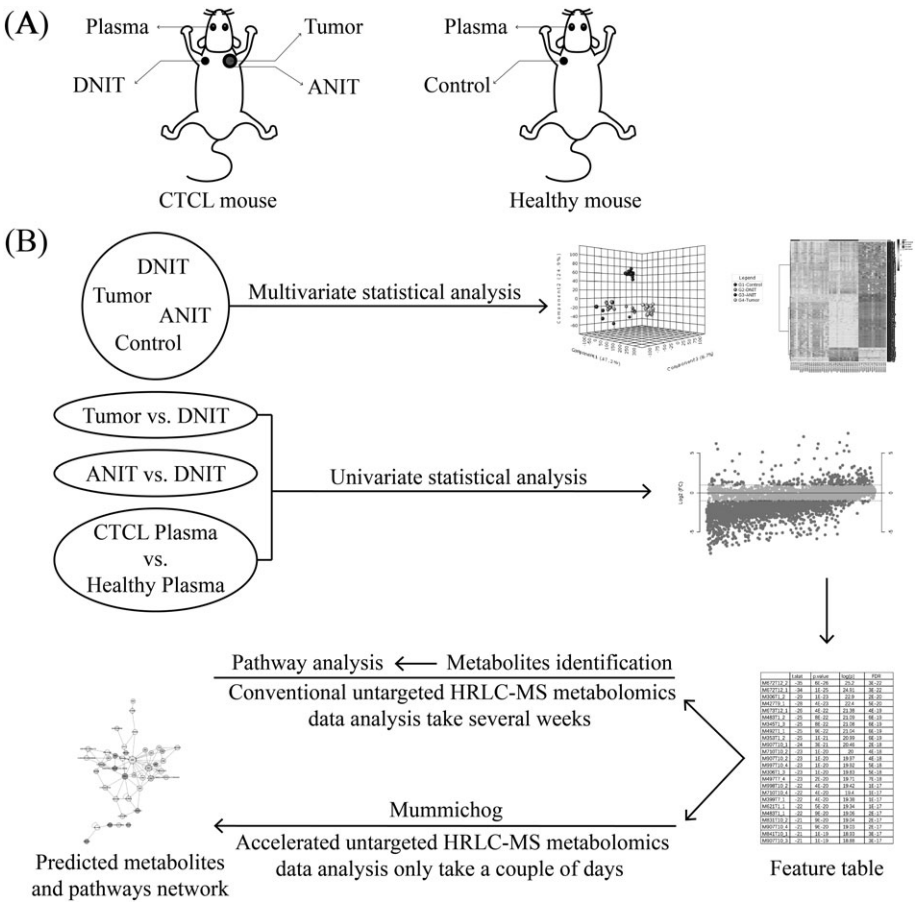

FIGURE 1 UHPLC-QTOF–based untargeted metabolomics workflow on cutaneous T-cell lymphoma (CTCL) xenograft mice tumor, skin, and plasma was accelerated by the application of Mummichog tool. A, CTCL xenograft mice and sample collection. B, Mummichog bypass the tedious metabolite identification to accelerate metabolomics study. ANIT, adjacent non-involved skin tissue; DNIT, distant non-involved skin tissue; HRLC-MS, high-resolution liquid chromatography–mass spectrometry

t = 25-27 minutes, decrease B from 100% to 1%. Data were collected by operating the mass spectrometer in positive and negative electrospray ionizations in centroid and profile mode, in full-scan range from 50 to 1000 *m/z*. Nitrogen was used as both cone gas and desolvation gas with a flow of 10 L/min. Nebulizer pressure was set at 40 psi. The desolvation temperature and capillary voltages were set at 350°C and 3500 V, respectively.

2.4 | Statistical data analysis

Raw mass spectra data were converted to mzDATA format files using Agilent MassHunter Qualitative Analysis B.06.00 software. Then the mzDATA files were uploaded to the XCMS Online (https://xcmsonline.scripps.edu) to preprocess to obtain the comma-separated values (csv) format peak intensity lists that contain *m/z*, retention time, and intensity of each peak. The further data statistics analysis was conducted by MetaboAnalyst 3.0 (http://www.metaboanalyst.ca) tool. The fully preprocessed data were then analyzed with multivariate analysis methods of principal component analysis (PCA) and partial least squares–discriminant analysis (PLS-DA). Heatmap was plotted to provide a visually intuitive overview of the different concentration changing patterns across different samples. After that, univariate analysis methods of fold change (FC) analysis and *t* test were applied between tumor and DNIT, ANIT, and DNIT, respectively, because the Mummichog analysis will use the *P* value and fold change value generated from univariate analysis (Figure 1B).

2.5 | Accelerated analysis strategy for metabolites and metabolic pathways prediction

Metabolic pathways and predicted metabolites in the pathways were analyzed using Mummichog 1.0.9 (http://mummichog.org) at the command line level. Mummichog is a program written in python for analyzing data from high-throughput, untargeted HRLC-MS metabolomics, bypassing the tedious and challenging metabolite identification (Figure 1B). It leverages the organization of metabolic networks to predict functional pathways directly from feature tables and generate a list of tentative metabolites annotations through functional activity analysis.[9] We input tab-delimited text files of peaks list with *m/z*, retain time, *P* value, and $\log_2$(FC) of 2-group analysis into Mummichog to conduct the pathways and module analysis. BioCyc (biocyc.org—human, mouse, fly, and yeast) mouse network model was selected, and the cut-off *P* value was set to .05 to generate a list of significant features, and all of the spectral features were treated as reference features in the computational algorithms of Mummichog. The analytical mode of mass spec was set to positive or negative, according the data source. Other options remained the default. Results from annotation, pathway analysis, and network module analysis were given. We then

used Cytoscape (http://www.cytoscape.org/) to visualize the results files of the metabolic pathways network and predicted metabolites. At last, the metabolites predicted by Mummichog were submitted to MetaboAnalyst to apply the receiver operating characteristic curve (ROC) test validation.

3 | RESULTS

3.1 | Raw data quality control and preprocessing

The uploaded positive mode UHPLC-QTOF raw data file of skin samples contained 52 samples by 9413 peaks data while negative mode data file containing 3115 peaks of the same number of samples. Finally, 4999 and 1868 peaks were retained after data filtering for positive and negative modes, respectively. Data were further normalized by sum followed by log transformation. These steps had individual features more comparable and exhibited a more normal or Gaussian distribution (Figure S1). Plasma samples UHPLC-QTOF raw data were also subjected to the same preprocessing steps. The summary of the data preprocessing results was shown in Table 1. The retention time drifts of quality control samples were less than 0.2 and 0.5 minutes in positive mode and negative mode, respectively, which indicated good reproducibility of our methodology.

3.2 | Skin samples were significantly distinguished by multivariate statistical analysis model

Multivariate statistical analysis methods were applied to obtain overview of the metabolome differences among the samples. The results provided intuitive reflection of the metabolism changing trends of skin tissue and plasma in the carcinogenesis of CTCL.

3D PCA plot (Figure S2) provided an overview of the various separation patterns among the most significant principal components (PCs). It showed a completely separation of tumor and other skin tissue samples. 2D PCA score plot (Figure 2A) further showed that the ANIT samples were separated from tumor and DNIT samples. A much better separation was obtained with PLS-DA model compared to PCA (Figure 2B). Generally, skin tissue samples were significantly distinguished as 3 classes: tumor, ANIT, and DNIT and control.

Moreover, the heatmap of top 500 *t* test significant features based on the positive mode data provided a visually intuitive overview of metabolites concentration changing trends among classes (Figure 3). It clearly showed that the concentration of metabolites concentration increased or decreased with the distribution of skins and the changing pattern varied among compounds. For example, a group of compounds in the upper part of the heatmap showed a significant abrupt decrease of concentration in tumor samples, while the middle part metabolites showed incremental concentration increase from control to tumor samples.

These results suggested that the DNIT and control samples had no significantly changed metabolic features. On the basis of this discovery, we only implement Mummichog analysis among tumor, ANIT, and DNIT classes since we can regard DNIT samples as control.

3.3 | Statistical validation of multivariate statistical analysis model

Cross-validation bar graph (Figure 2C) is used to determine the optimal number of components needed to build the PLS-DA model. There are 3 common performance measures—the sum of squares captured by the model (R2), the cross-validated R2 (also known as Q2), and the prediction accuracy (accuracy). The default criterion is Q2, which indicated (as marked by a red star) that a 5-component model was the best both for positive mode and negative mode analyses, since Q2 of PC5 were highest among all the PCs based on the positive mode data (Table 1). The result of permutation test of PLS-DA for positive mode data was shown in Figure 2D. It is clear that the statistics based on the original data is very different from the statistics distribution calculated from permutated data. The *P* value is .005 in 1000 permutations means that just 5 in 1000 permutations will the permutated data yielded a better performance than the original data, which was considered very significant. The negative mode data of tissue samples also showed similar statistical data analysis results (Supporting Information).

3.4 | Elevated GLT and decreased adenosine monophosphate were the most essential metabolic features of CTCL tumor and its adjacent skins

The metabolites prediction and pathways analysis were based on univariate statistical analysis. Summary of the univariate statistical analysis was shown in Table 2. Mummichog uses the reference and significant features to compute significant pathways and modules to generate a list of predicted metabolites and metabolic networks (Figure 4). The complete list of metabolits predicted by Mummichog was provided in Table S1.

Elevated L-glutamate (GLT) and decreased adenosine monophosphate (AMP) were the most significant feature of CTCL tumor and ANIT (Figure 4A,B). GLT-related metabolic shifts included significant aberrant level of amino acids. Adenosine monophosphate level decrease was associated with changes of amino acids and nucleotides. These metabolites mostly involved in the metabolic pathways of tRNA charging pathway (Table 3). The other important pathway

TABLE 1 Summary of data preprocessing and multivariable statistical data analysis

	Skin		Plasma	
	Positive	Negative	Positive	Negative
Number of peaks in raw data	9513	3115	7189	2997
Number of peaks after data filtering and normalization	4999	1868	4313	1798
PLS-DA cross-validation details	accuracy = 0.962 R2 = 0.996 Q2 = 0.937	accuracy = 1.0 R2 = 0.998 Q2 = 0.973	accuracy = 0.806 R2 = 0.998 Q2 = 0.421	accuracy = 1.0 R2 = 0.998 Q2 = 0.790

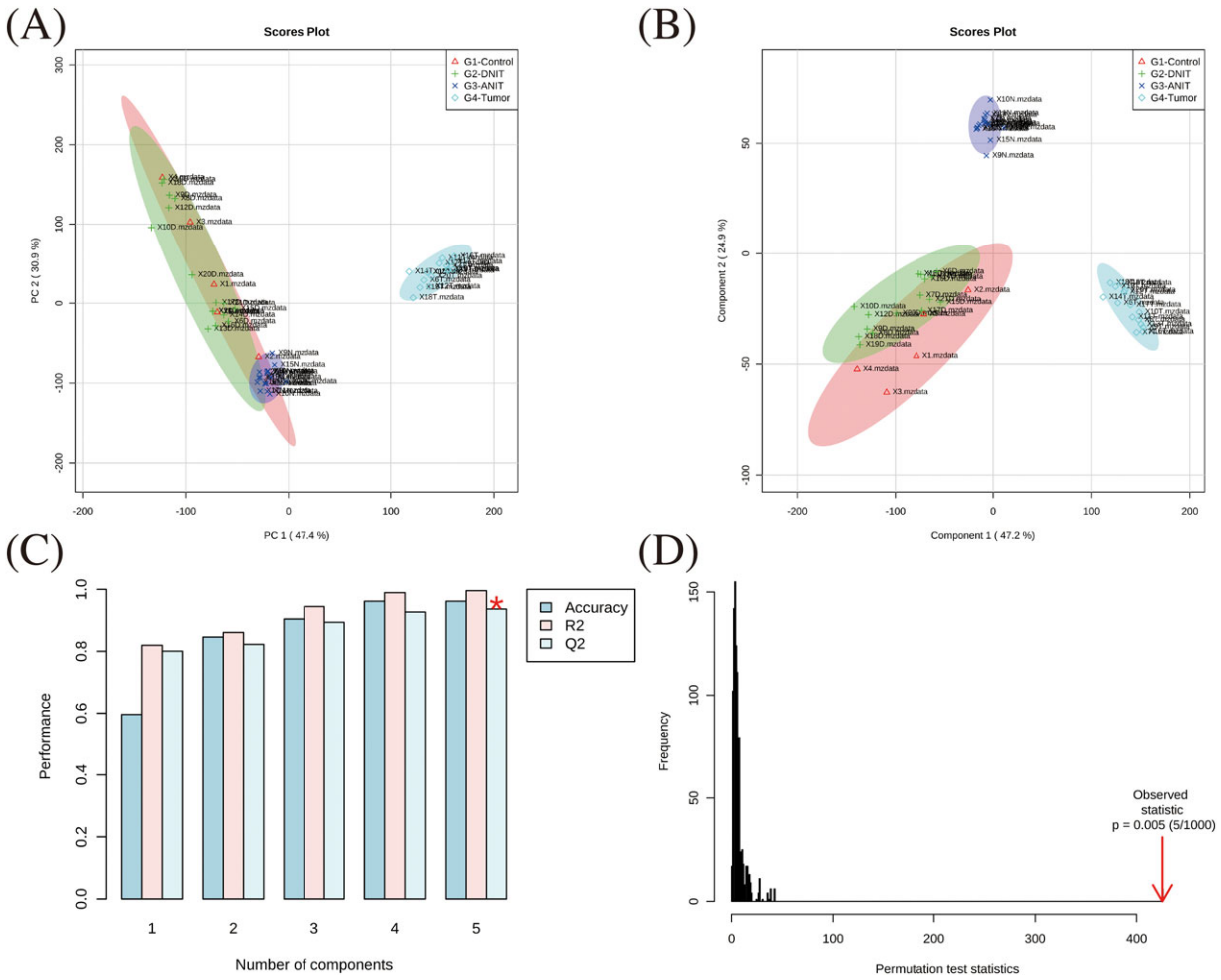

FIGURE 2 Multivariate statistical analysis of tumor, adjacent non-involved skin tissue (ANIT), distant non-involved skin tissue (DNIT), and control samples in positive mode analysis. A, 2D scores plot between the selected PCs of PCA model. B, 2D scores plot between the selected PCs of partial least squares-discriminant analysis (PLS-DA) model, C, Cross-validation bar graph used to determine the optimal number of components (marked by the red star) needed to build the PLS-DA model. D, PLS-DA model validation by permutation tests based on separation distance

was bile acid biosynthesis in which metabolites of taurine, taurocholate, cholesterol, and 7-α-hydroxycholesterol involved.

The metabolic pathways differed in both tumor and ANIT, indicated that they are the most essential metabolic signatures of tumor in CTCL (Figure 4D).

3.5 | Unique metabolism changes in ANIT reflected the progress of carcinogenesis

On the other hand, tumor and ANIT showed different metabolic changing characteristics (Figure 4A,B), which suggested that these changes may play an important role in the early stage of carcinogenesis.

Sharply elevated cytidine-5′-triphosphate (CTP) was the most significant changed compound in ANIT, which involved in the pathways of pyrimidine deoxyribonucleotides de novo biosynthesis and cytidine monophosphate-*N*-acetylneuraminate biosynthesis (Figure 4A). Biosynthesis of prostaglandins was enhanced by the aberrant high level of prostaglandin F2α, prostaglandin F2α, and arachidonate. Metabolites acetoacetyl-CoA and (S)-3-hydroxy-3-methylglutaryl-CoA were involved in the mevalonate pathway. Tryptophan degradation was enhanced by the increased L-kynurenine and decreased anthranilate.

These metabolic pathway changes (Table 3) occurred in the adjacent skin area of tumor, which indicated that they are important signals in the development of CTCL and have potentials in the diagnosis of early stage CTCL.

3.6 | Sharply elevated PRPP marked the final state of tumor in CTCL

Sharply elevated 5-phospho-α-D-ribose 1-diphosphate (PRPP) was a crucial metabolite in tumor of CTCL, which affected the metabolites of purines, pyrimidines, nucleosides, and nucleotides (Figure 4B). These metabolites based aberrant metabolic pathways focused on purine and pyrimidine metabolism, purine ribonucleosides degradation to ribose-1-phosphate, (deoxy) ribose phosphate degradation, and pyridine nucleotide cycling (Table 3), which marked the final metabolic state associated with the CTCL.

3.7 | High level of sphingosine-1-phosphte and decreased corticosterone and in plasma of CTCL mice

The rewrote metabolic pathways networks in plasma of CTCL mice were shown in Figure 4C. The distribution of metabolites was more

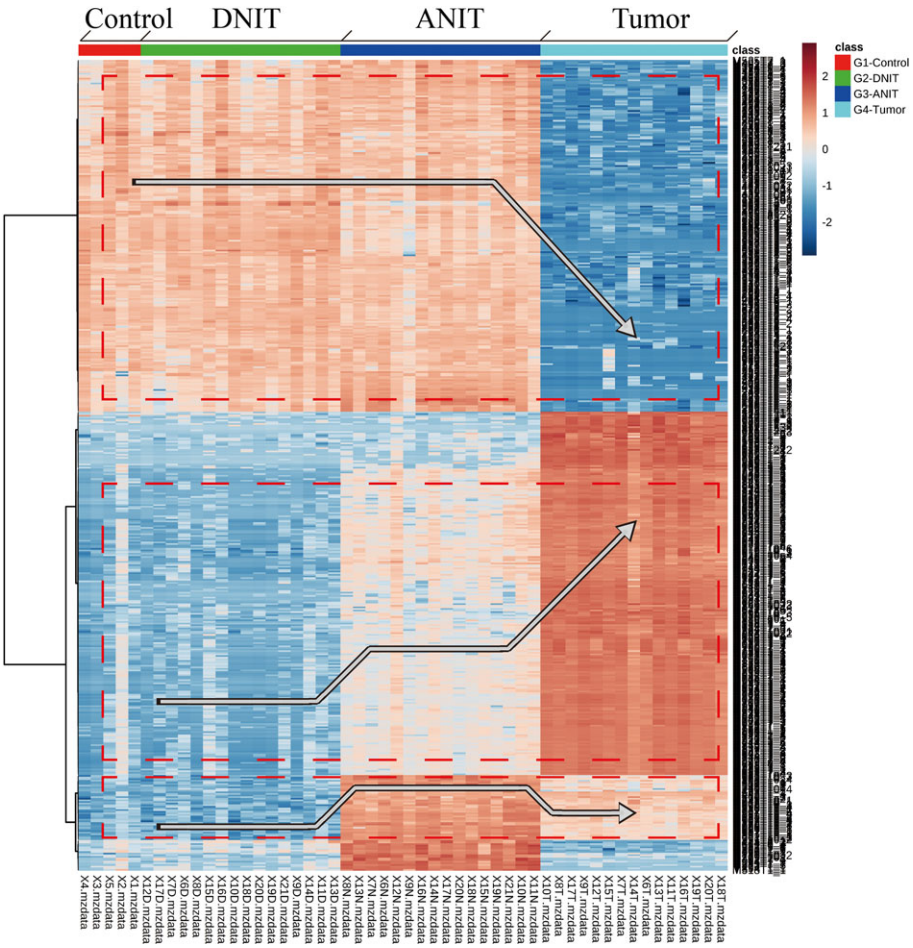

FIGURE 3 Heatmap of top 500 significant features showed their concentration changing patterns. ANIT, adjacent non-involved skin tissue; DNIT, distant non-involved skin tissue

TABLE 2 Summary of univariate statistical data analysis and Mummichog analysis results

	Tumor		ANIT		Plasma	
	Positive	Negative	Positive	Negative	Positive	Negative
Number of peaks in raw data	9409	3099	9404	3113	7189	2997
Number of peaks after data filtering and normalization	4999	1859	4999	1867	4313	1798
Number of peaks selected as significant features ($P < .05$)	3895	1329	3874	959	587	454
Number of metabolites predicted by Mummichog	48	6	59	2	49	10

Abbreviation: ANIT, adjacent non-involved skin tissue.

decentralized in the metabolic network of plasma, which showed a huge metabolism difference between plasma and skins. The most significantly changed pathways were downregulated biosynthesis of corticosteroids, upregulated sphingosine metabolism, glutathione-mediated detoxification, and ceramide biosynthesis (Table 3), which were not observed in skin samples. The complete lists of metabolic pathways predicted by Mummichog were in shown in the Supporting Information.

3.8 | Correlation analysis with tumor size and ROC test of S1P, CTP, and PRPP

The Pearson correlation coefficients (ρ) of tumor size and significantly changed metabolites levels (peak area) were computed (Figure 5A). The results showed that tumor size was strongly, positively correlated with PRPP (ρ = 0.80) in tumor tissues. Sphingosine-1-phosphate (S1P) also had positively correlation (ρ = 0.64) with tumor size in tumor subjects' plasma. In ANIT samples, CTP was most significantly positively correlated with tumor size (ρ = 0.83). PRPP and CTP had no significant correlation with tumor size in the DNIT samples. These results demonstrated the interaction of pentose phosphate pathway, and nucleotides metabolism had great influence in the progression of CTCL cancerization. The ROC values of S1P, CTP, and PRPP, which are the most significant metabolites of plasma, ANIT, and tumor class according to Mummichog, were shown in Figure 5B. Herein, we choose the M + H or M form of these 3 compounds (Table 4) to show their ROC curve. The area under curve of them were 0.85, 0.988, and 1.0, respectively. The *P* value of them were .026, 4.98E-06, and

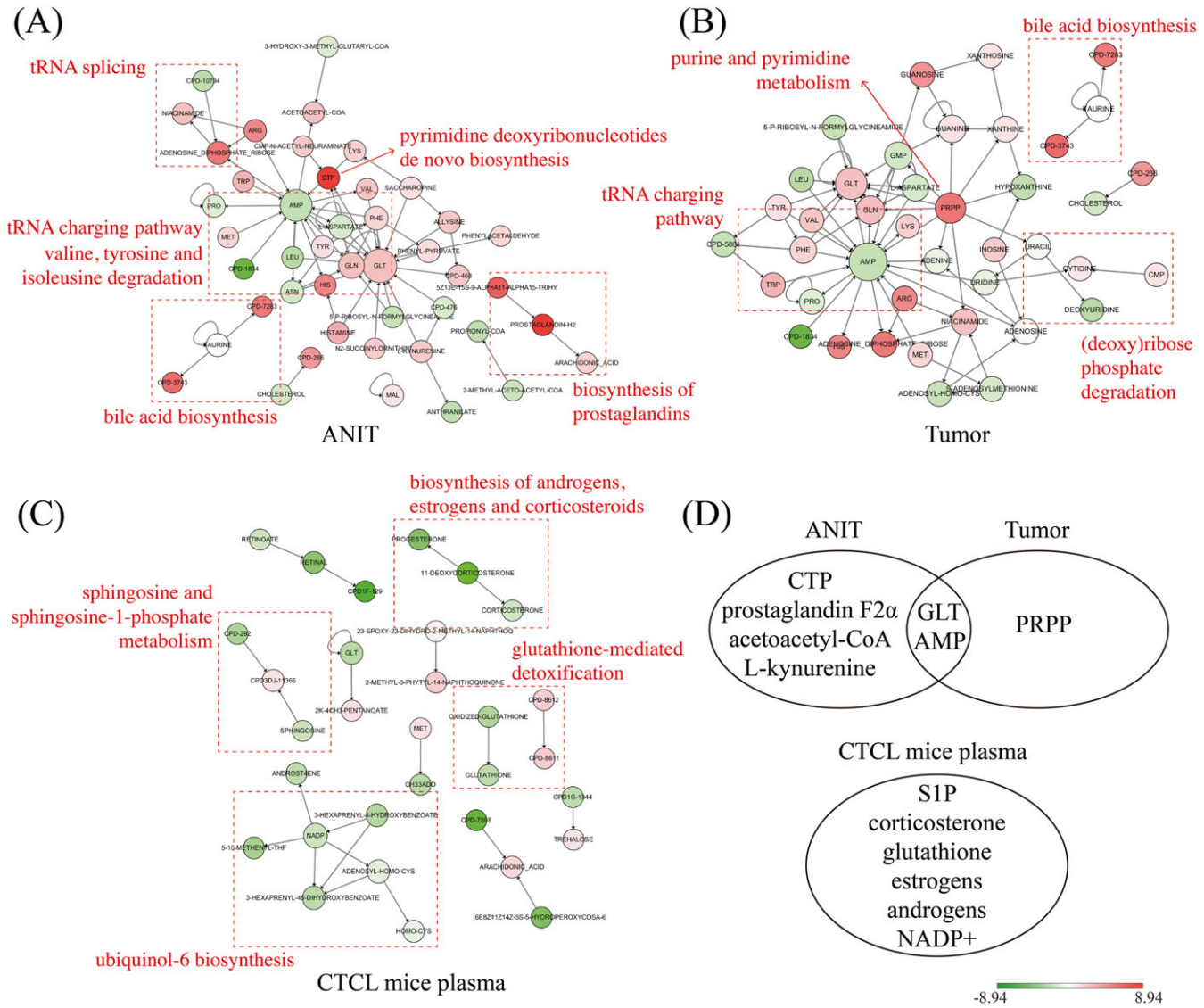

FIGURE 4 Networks of activity pathways generated from the analysis of Mummichog and visualized via Cytospace. Metabolites are colored green (concentration decrease) or red (concentration increase), and the size and color intensity represents the connectivity of the metabolite in the networks and magnitude of fold change. A, Activity pathways networks of adjacent non-involved skin tissue (ANIT). B, Activity pathways networks of tumor. C, Activity pathways networks of plasma. D, Venn diagram of the most significant metabolites of ANIT, tumor, and plasma class. AMP, adenosine monophosphate; CTCL, cutaneous T-cell lymphoma; CTP, cytidine-5′-triphosphate; DNIT, distant non-involved skin tissue; GLT, L-glutamate; NADP, nicotinamide adenine dinucleotide phosphate; PRPP, 5-phospho-α-D-ribose 1-diphosphate; S1P, sphingosine-1-phosphate

2.99E-13. Details of the ROC curve of these 3 compounds and other compounds predicted by Mummichog were shown in the Supporting Information.

4 | DISCUSSION

Metabolomics was applied in this study to compare tumor tissues and adjacent healthy skin tissues to explore the disease progression of CTCL. Metabolomics analyses have concerned a range of cancers including lung, colorectal, bladder, breast, gastric, oesophageal, and thyroid, among others, for discovery of biomarkers and personal medicine.[10] For example, the glutamate-to-glutamine ratio represents new biomarker that was increased in 88% of hormone receptor negative (HR−) tumors and 56% of hormone receptor positive (HR +) tumors compared to normal breast tissues.[11] Metabolomics profiling of paired adipose samples of colorectal cancers patients showed that compared with subcutaneous adipose tissue, visceral adipose tissue displayed elevated markers of inflammatory lipid metabolism, free arachidonic acid, phospholipases, and prostaglandin synthesis-related enzymes.[12] In our study, PRPP, CTP, and S1P were associated with CTCL progression in tumor, skin tissues, and plasma, respectively.

PRPP played a pivotal role in the metabolic changing of CTCL according to our study. PRPP is used in the biosynthesis of purine and pyrimidine nucleotides, amino acids histidine and tryptophan, and cofactors nicotinamide adenine dinucleotide.[13] As a critical intermediate metabolite between carbon metabolism and nitrogen

TABLE 3 Three most significant pathways for each class uncovered by Mummichog in positive mode

Class	Pathway	*P* value	Overlap Compounds (Name)
Plasma	Sphingosine and sphingosine-1-phosphate metabolism	.0040	2-trans-Hexadecenal; sphingosine-1-phosphate; sphingosine; palmitaldehyde
	Glutathione-mediated detoxification	.0042	CoA; glutathione; L-glutamate
	Ceramide biosynthesis	.0042	CoA; palmitoyl-CoA; 3-dehydrosphinganine
ANIT	tRNA charging pathway	.0005	L-aspartate; L-isoleucine; L-valine; L-glutamine; L-lysine; AMP; L-proline; L-phenylalanine; L-methionine; L-histidine; L-leucine; L-arginine; L-tryptophan; L-glutamate; L-asparagine; L-tyrosine
	Nicotine degradation III	.0011	3-Pyridylacetate; UDP; UDP-D-glucuronate; 4-(3-pyridyl)-butanoate; 4-(3-pyridyl)-3-butenoate; trans-3-hydroxycotinine-glucuronide; norcotinine; 4-hydroxy-4-(3-pyridyl)-butanoate; 4-oxo-4-(3-pyridyl)-butanoate; cotinine-glucuronide; NADP+; cotinine methonium ion; cotinine
	Pyrimidine deoxyribonucleotides de novo biosynthesis I	.0023	5,10-Methylenetetrahydropteroyl mono-L-glutamate; UDP; CTP; dUMP; 7,8-dihydrofolate monoglutamate; dUTP; dTTP; dUDP
Tumor	tRNA charging pathway	.0106	L-Cysteine; L-aspartate; L-isoleucine; L-valine; L-glutamine; L-lysine; AMP; L-proline; L-phenylalanine; L-methionine; L-histidine; L-leucine; L-arginine; L-tryptophan; L-glutamate; L-asparagine; L-tyrosine
	Bile acid biosynthesis, neutral pathway	.0189	Taurocholate; glycochenodeoxycholate; (25R)-5-β-cholestane-3-α,7-α,12-α,26-tetraol; (25R)-5-β-cholestane-3-α,7-α,26-triol; propanoyl-CoA; (25R)-3-α,7-α,12-α-trihydroxy-5-β-cholestan-26-oate; (25R)-3-α,7-α,12-α-trihydroxy-5-β-cholestan-26-al; (25R)-3-α,7-α-dihydroxy-5-β-cholestanate; taurochenodeoxycholate; (25R)-3-α,7-α-dihydroxy-5-β-cholestan-26-al; glycocholate; 7-α-hydroxy-5-β-cholestan-3-one; 5-β-cholestane-3-α,7-α-diol; 7-α,12-α-dihydroxy-5-β-cholestan-3-one; cholesterol; 7-α-hydroxycholesterol; AMP; taurine; NADP+; 7-α,12-α-dihydroxycholest-4-en-3-one; 5-β-cholestane-3-α,7-α,12-α-triol
	Purine and pyrimidine metabolism	.0216	dTMP; 7,8-dihydrofolate monoglutamate; GMP; uracil; adenine; adenosine; guanosine; cytidine; guanine; 5-phospho-α-D-ribose 1-diphosphate; uridine; AMP; dTDP; 5,10-methylenetetrahydropteroyl mono-L-glutamate; CMP

Abbreviations: ANIT, adjacent non-involved skin tissue; AMP, adenosine monophosphate; CoA, coenzyme A; CTP, cytidine-5′-triphosphate; dTDP, deoxythymidine diphosphate; dTMP, deoxythymidine monophosphate; dTTP, deoxythymidine triphosphate; dUDP, deoxyuridine diphosphate; dUMP, deoxyuridine monophosphate; dUTP, deoxyuridine triphosphate; GMP, guanosine monophosphate; NAD, nicotinamide adenine dinucleotide; UDP, uridine diphosphate.

sources, an increase in PRPP levels may be sufficient to govern the overall nucleotide biosynthetic rate of cells. A single rate-limiting enzyme, phosphoribosyl pyrophosphate synthetase 2, that promoted increased PRPP levels and nucleotide biosynthesis is crucial for transcription factor Myc-driven tumorigenesis.[14] Therefore, more attention would be paid on PRPP-based metabolic pathways and enzyme, such as PRPP synthase, as a potential therapeutic target in CTCL.

More importantly, the CTP levels in ANIT reflect the carcinogenesis progress in CTCL, which may act as a crucial biomarker in the distinguishing of benign disorders and tumor. CTP is a critical intermediate metabolite in the pyrimidine metabolism, which is also associated with pentose phosphate pathway via PRPP. Several cytidine-related kinase and enzyme that involved in the salvage pathway of pyrimidine-nucleotide biosynthesis, such as cytidine monophosphate kinase,[15] uridine-cytidine kinase 2,[16] and cytidine deaminase, were reported to be overexpressed or downregulated in tumor cells. For example, cytidine deaminase that catalyzes the irreversible hydrolytic deamination of cytidine to uridine, was found expression downregulated in about 60% of cancer cells and tissues.[17] In our study, the levels of uridine were also observed downregulated in CTCL tumor tissues while CTP was upregulated. Thus, the disorders in pyrimidine salvage pathway may play a prevalent role in progress of CTCL. The metabolic reprogramming of PRPP in tumor tissues may cause the disturbance of cytidine and uridine metabolic homeostasis in ANIT. Accumulative CTP in ANIT exerts positive feedback on the PRPP level and leads to CTCL development.

Blood could play a messenger role in CTCL's spread to surrounding healthy skin tissues. Our study found a very significant and important systematic shift in sphingolipid metabolism of aberrant high level of S1P in CTCL plasma samples. The correlation of S1P pathways with cancer have been reported widely. An altered ceramide/S1P balance is an important feature of human cancers. Increased S1P content in glioblastoma tissue compared to normal gray matter was significantly correlated with increased sphingosine kinase 1.[18] Sphingosine kinase 1 also played crucial role in the metabolic shift known as the Warburg effect in ovarian cancer cells by induction of aerobic glycolysis and affecting metabolic pathways that support the biosynthesis of macromolecules in tumor cells.[19] Elevated S1P in blood could speed up the glycolytic rate, which thus produces more PRPP in tumor cells to promote the tumor proliferation in CTCL.

High-throughput omics analysis can be used not only to verify the predecessor's clinical and histopathological diagnosis practices but also to provide novel discoveries about pathogenesis hypothesis and carcinogenesis mechanism. The significantly changed metabolites not only are the results of disease but also play a functional role in the development of disease. A hypothetical metabolites function mechanism based on our metabolomics study was shown in Figure 6. How the metabolic pathways uncovered by presented study involve in the carcinogenesis progress such as proliferation, apoptosis resistance, and immune-related responses of CTCL will be an interesting study in the next.

Last but not least, the applied metabolomics data analysis strategy "Mummichog" herein presented a greatly accelerated interpretation

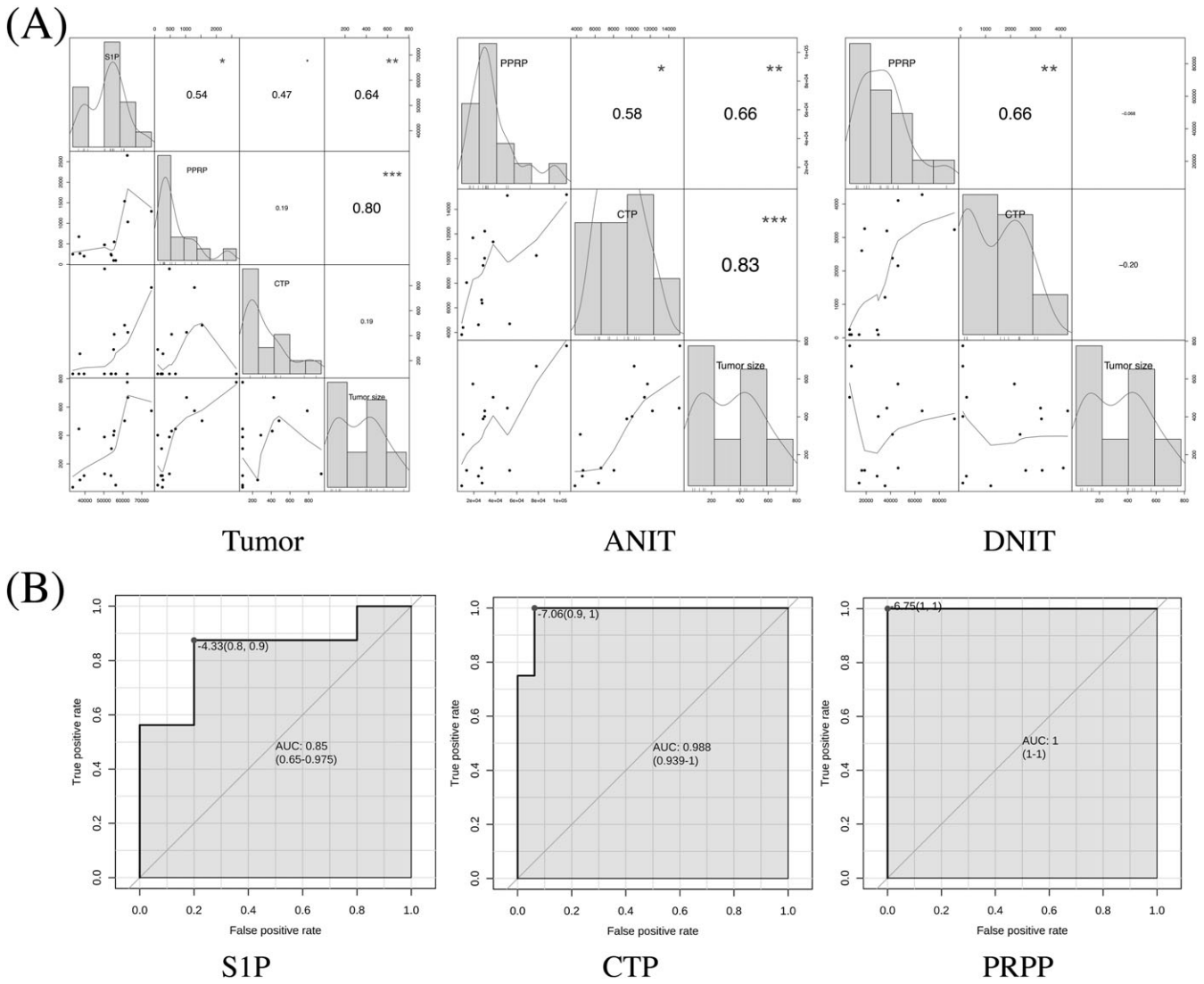

FIGURE 5 A, Correlation analysis of tumor size and 5-phospho-α-D-ribose 1-diphosphate (PRPP), cytidine-5′-triphosphate (CTP), and sphingosine-1-phosphate (S1P) in tumor, adjacent non-involved skin tissue (ANIT), and distant non-involved skin tissue (DNIT) samples. B, Receiver operating characteristic curve test for S1P, CTP, and PRPP

TABLE 4 Mass-to-charge ratio of S1P, CTP, and PRPP and their match forms

Class	Compound ID	Name	Input *m/z*	Match form	MW
Plasma	S1P	Sphingosine-1-phosphate	380.2588	M + H[1+]	379.2488
	S1P	Sphingosine-1-phosphate	381.2621	M(C13) + H[1+]	379.2488
	S1P	Sphingosine-1-phosphate	402.2416	M + Na[1+]	379.2488
ANIT	CTP	CTP	551.9763	M + HCOONa[1+]	482.9845
	CTP	CTP	521.9503	M + K[1+]	482.9845
	CTP	CTP	437.9903	M-HCOOH + H[1+]	482.9845
Tumor	PRPP	5-Phospho-α-D-ribose 1-diphosphate	412.9396	M + Na[1+]	389.9518
	PRPP	5-Phospho-α-D-ribose 1-diphosphate	389.9513	M[1+]	389.9518

Abbreviations: ANIT, adjacent non-involved skin tissue; CTP, cytidine-5′-triphosphate; PRPP, 5-phospho-α-D-ribose 1-diphosphate; S1P, sphingosine-1-phosphate.

solution for HRLC-MS analysis. This tool had been cited in several metabolomics review articles.[20-22] It also had been integrated in the XCMS online workflow to operate directly on the entire metabolic features table.[23] Mummichog tool considerably improves the efficiency of metabolites annotation and pathways analysis in our study. System biological solutions and novel statistical algorithms of Mummichog benefit the HRLC-MS data interpretation, especially for the HRLC-MS that lack sufficient spectral library, which thus leads to the lengthy conventional workflow retarded by the tedious of metabolites identification. The accelerated data analysis workflow could help to further dig the information generated by HRLC-MS metabolomics platforms and provide more clues for biology validation in the future.

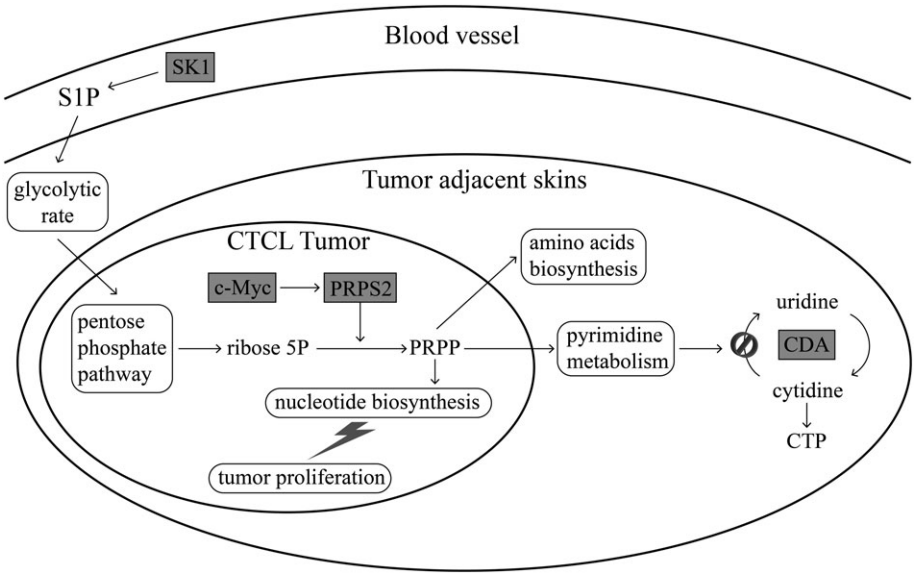

FIGURE 6 Hypothetical metabolic pathways and biological signaling interaction mechanism in cutaneous T-cell lymphoma (CTCL). CDA, cytidine deaminase; CTP, cytidine-5′-triphosphate; PRPP, 5-phospho-α-D-ribose 1-diphosphate; S1P, sphingosine-1-phosphate

5 | CONCLUSION

We applied an accelerated metabolomics tool Mummichog for data analysis to conduct UHPLC-MS–based untargeted metabolomics on CTCL xenograft mice. Our study showed that the metabolic reprogramming of PRPP in tumor tissues cause the disturbance of cytidine and uridine metabolic homeostasis in ANIT. Accumulative CTP in ANIT then exert positive feedback on the PRPP level and lead to CTCL for further development. These metabolites and associated pathways involve in the "preneoplastic" state and carcinogenesis development of CTCL thus are crucial in early stage clinical diagnosis and can provide new insights for further understanding of pathogenesis in CTCL.

ACKNOWLEDGEMENTS

This study was funded by Natural Science Foundation of China (KRF301100). The authors declare no conflict of interest. All applicable international, national, and/or institutional guidelines for the care and use of animals were followed.

ORCID

Yunqiu Yu http://orcid.org/0000-0002-5629-8753

REFERENCES

1. DeSimone JA, Sodha P, Ignatova D, Dummer R, Cozzio A, Guenova E. Recent advances in primary cutaneous T-cell lymphoma. *Curr Opin Oncol*. 2015;27:128-133.
2. Chung CG, Poligone B. Cutaneous T cell lymphoma: an update on pathogenesis and systemic therapy. *Curr Hematol Malig Rep*. 2015; 10:468-476.
3. Scarisbrick JJ, Prince HM, Vermeer MH, et al. Cutaneous Lymphoma International Consortium Study of outcome in advanced stages of mycosis fungoides and Sézary syndrome: effect of specific prognostic markers on survival and development of a prognostic model. *J Clin Oncol*. 2015;33:3766-3773.
4. Moriarty B, Whittaker S. Diagnosis, prognosis and management of erythrodermic cutaneous T-cell lymphoma. *Expert Rev Hematol*. 2015;8:159-171.
5. Kirsch IR, Watanabe R, O'Malley JT, et al. TCR sequencing facilitates diagnosis and identifies mature T cells as the cell of origin in CTCL. *Sci Transl Med*. 2015;7:308ra158.
6. Litvinov IV, Netchiporouk E, Cordeiro B, et al. The use of transcriptional profiling to improve personalized diagnosis and management of cutaneous T-cell lymphoma (CTCL). *Clin Cancer Res*. 2015;21:2820-2829.
7. Ion A, Popa IM, Papagheorghe LM, et al. Proteomic approaches to biomarker discovery in cutaneous T-cell lymphoma. *Dis Markers*. 2016;2016: 9602472.
8. Zhou QY, Wang YL, Li X, et al. Metabolomics investigation of cutaneous T cell lymphoma based on UHPLC-QTOF/MS. *Asian Pac J Cancer Prev*. 2014;15:5417-5421.
9. Li S, Park Y, Duraisingham S, et al. Predicting network activity from high throughput metabolomics. *PLoS Comput Biol*. 2013;9:e1003123.
10. Armitage EG, Ciborowski M. Applications of metabolomics in cancer studies. *Adv Exp Med Biol*. 2017;965:209-234.
11. Budczies J, Denkert C. Tissue-based metabolomics to analyze the breast cancer Metabolome. *Recent Results Cancer Res*. 2016; 207:157-175.
12. Liesenfeld DB, Grapov D, Fahrmann JF, et al. Metabolomics and transcriptomics identify pathway differences between visceral and subcutaneous adipose tissue in colorectal cancer patients: the ColoCare study. *Am J Clin Nutr*. 2015;102:433-443.
13. Hove-Jensen B, Andersen KR, Kilstrup M, Martinussen J, Switzer RL, Willemoes M. Phosphoribosyl diphosphate (PRPP): biosynthesis, enzymology, utilization, and metabolic significance. *Microbiol Mol Biol Rev*. 2017;81:1-83.
14. Cunningham JT, Moreno MV, Lodi A, Ronen SM, Ruggero D. Protein and nucleotide biosynthesis are coupled by a single rate-limiting enzyme, PRPS2, to drive cancer. *Cell*. 2014;157:1088-1103.
15. Zhou D, Zhang L, Sun W, et al. Cytidine monophosphate kinase is inhibited by the TGF-beta signalling pathway through the upregulation of miR-130b-3p in human epithelial ovarian cancer. *Cell Signal*. 2017;35:197-207.
16. Shen G, He P, Mao Y, et al. Overexpression of uridine-cytidine kinase 2 correlates with breast cancer progression and poor prognosis. *J Breast Cancer*. 2017;20:132-141.

17. Mameri H, Bieche I, Meseure D, et al. Cytidine deaminase deficiency reveals new therapeutic opportunities against cancer. *Clin Cancer Res*. 2017;23:2116-2126.
18. Abuhusain HJ, Matin A, Qiao Q, et al. A metabolic shift favoring sphingosine 1-phosphate at the expense of ceramide controls glioblastoma angiogenesis. *J Biol Chem*. 2013;288:37355-37364.
19. Bernacchioni C, Ghini V, Cencetti F, et al. NMR metabolomics highlights sphingosine kinase-1 as a new molecular switch in the orchestration of aberrant metabolic phenotype in cancer cells. *Mol Oncol*. 2017;11:517-533.
20. Johnson CH, Ivanisevic J, Siuzdak G. Metabolomics: beyond biomarkers and towards mechanisms. *Nat Rev Mol Cell Biol*. 2016;17:451-459.
21. Barnes S, Benton HP, Casazza K, et al. Training in metabolomics research. II. Processing and statistical analysis of metabolomics data, metabolite identification, pathway analysis, applications of metabolomics and its future. *J Mass Spectrom*. 2016;51:535-548.
22. Johnson CH, Ivanisevic J, Benton HP, Siuzdak G. Bioinformatics: the next frontier of metabolomics. *Anal Chem*. 2015;87:147-156.
23. Huan T, Forsberg EM, Rinehart D, et al. Systems biology guided by XCMS online metabolomics. *Nat Methods*. 2017;14:461-462.

SUPPORTING INFORMATION

Additional Supporting Information may be found online in the supporting information tab for this article.

How to cite this article: Le Y, Shen X, Kang H, et al. Accelerated, untargeted metabolomics analysis of cutaneous T-cell lymphoma reveals metabolic shifts in plasma and tumor adjacent skins of xenograft mice. *J Mass Spectrom*. 2018;172–182. https://doi.org/10.1002/jms.4048